Research Article

Pu Jiang, Zujian Chen, Na Zhang, Kun Gao*

A zinc oxide–tin oxide–nerolidol hybrid nanomaterial: Efficacy against esophageal squamous cell carcinoma

https://doi.org/10.1515/chem-2024-0076
received April 20, 2024; accepted July 6, 2024

Abstract: The sixth most common cancer in the world, esophageal cancer, requires aggressive treatment such as surgery, chemotherapy, radiotherapy, and immunotherapy. Phytochemicals and medicinal plants are being used in the green synthesis of nanoparticles. Our study aimed to synthesize ZnO–SnO_2 nerolidol nanocomposite and study its effects on esophageal squamous cell carcinoma cells. UV spectroscopy showed significant absorbance at 288 nm, transmission electron microscopy and DLS showed spherical shapes, and transmission electron microscopy also showed 108 nm average diameters. The ZnO–SnO_2 nerolidol nanocomposite was also investigated using energy-dispersive X-ray analysis, Fourier transform infrared spectroscopy, photoluminescence, and field emission scanning electron microscopy. A cytotoxic effect was observed against KYSE-150 cells with an IC_{50} concentration of 14.9 µg/mL. The ZnO–SnO_2 nerolidol nanocomposite inhibited cancer cell proliferation in KYSE-150 cells and enhanced apoptosis by altering its mitochondrial membrane potential. The ZnO–SnO_2 nerolidol nanocomposite also enhanced oxidative stress, leading to a decrease in superoxide dismutase, catalase, and glutathione and an increase in lipid peroxidation. Ultimately, ZnO–SnO_2 nerolidol nanocomposite enhanced the caspase cascade by inducing caspases 3, 8, and 9 in KYSE-150 cells. On the whole, we suggest that the ZnO–SnO_2 nerolidol nanocomposite can be an effective treatment strategy against esophageal squamous cell carcinoma in KYSE-150 cells. However, understanding molecular circuits is still warranted.

Keywords: ZnO, SnO_2, nerolidol, apoptosis, caspases

1 Introduction

Esophageal cancer (EC) is ranked the ninth most prevalent cancer worldwide and is the sixth leading cause of death worldwide. It is a highly aggressive malignant tumor and comprises two different diseases, esophageal adenocarcinoma and esophageal squamous cell carcinoma, affecting more than 400,000 people worldwide every year [1,2]. Among them, esophageal squamous cell carcinoma is the most common histological type of EC, constituting 85.79%, while esophageal adenocarcinoma comprises 11% and others include 3.21% [3]. The therapeutic strategy for early-stage EC is surgery, and the other conventional treatment methods include chemotherapy, radiotherapy, neoadjuvant chemotherapy, and chemoradiotherapy. The 5-year survival rate for EC is around 20% [4].

Additionally, the combination of immune checkpoint inhibitors with chemotherapy is the treatment for advanced esophageal squamous cell carcinoma. However, the therapy response for combination therapy ranges from 16.7 to 58.3% [5]. Thus, several treatment strategies are inadequate or lead to several side effects. The alternative treatment strategy that is receiving much interest is the use of phytochemicals, which show activity against various metabolic diseases and cancers. Despite their efficacy, the requirement of nano-sized, green-synthesized nanoparticles (NPs) using phytochemicals or medicinal plants has been of keen interest to scientists [6].

Nerolidol (peruviol, 3,7,11-trimethyl-1,6,10-dodecatrien-3-ol), a sesquiterpene alcohol, is found in the essential oils

* **Corresponding author: Kun Gao,** Department of Thoracic Surgery, The Fourth Hospital of Hebei Medical University, No. 12 Jiankang Road, Shijiazhuang, Hebei, 050000, China, e-mail: 2078385814@139.com
Pu Jiang: Department of Thoracic Surgery, The Fourth Hospital of Hebei Medical University, No. 12 Jiankang Road, Shijiazhuang, Hebei, 050000, China
Zujian Chen: Department of Thoracic Surgery, Linxi County People's Hospital, New Campus of Linxi County People's Hospital, Xingtai, Xingtai Linxi County, 054900, China
Na Zhang: Department of Radiation Oncology, The Fourth Hospital of Hebei Medical University, No. 12 Jiankang Road, Shijiazhuang, Hebei, 050000, China

of various plants [7] and reported to possess various antioxidant, anti-microbial, anti-inflammatory and anti-tumor potentials [8]. Nerolidol was reported to show poor oral bioavailability, hydrophobicity, and failure to get steady-state plasma concentration [9]. Thus, the development of efficient NPs might be a promising strategy to facilitate efficient delivery and enhanced bioavailability against cancer and is essentially needed [8].

Green synthesis uses environmentally compatible materials like bacteria, fungi, and plants to synthesize NPs, such as zinc oxide nanoparticles (ZnO NPs) [10]. These NPs are easily prepared, inexpensive, and safe and are used in various biomedical sectors due to their high electron mobility, wide band gap, and elevated exciton energy [11]. ZnO NPs have been used as anti-cancer agents due to their cytotoxic activity against various cancers, including triple-negative breast cancer, MCF7 breast cancer, lung adenocarcinoma, bladder cancer, oral cancer, liver cancer cells, and chronic myeloid leukemia [12,13]. However, there are limited studies on the bio-activity of chemically synthesized ZnO NPs on A431 cells and the effect of time of NaOH addition in the reaction mixture [14,15]. In recent years, the tendency to use NPs with anticancer properties is increasing. Among these, tin oxide (SnO_2) NPs have been identified as one of the most effective anticancer compounds due to their appropriate efficacy and potential compatibility at low concentrations [16,17]. For example, it has been shown that SnO_2 NPs show potential albumin binding and anticancer effects activity against MCF-7 cells. Also, it has been shown that SnO_2 NPs can be developed as promising anticancer platforms against cervical carcinoma [18].

The novelty of the study shows that ZnO/SnO_2 and nerolidol nanocomposite are a promising treatment for esophageal squamous cell carcinoma, particularly against KYSE-150 cells. It enhances anticancer efficacy, improves drug delivery, and increases cellular uptake, reducing side effects and providing a versatile treatment platform. The small size and surface modification of the nanocomposite facilitate better penetration and uptake by cancer cells.

The study aims to establish a novel nanocomposite system for the effective delivery of nerolidol and evaluate its potential as a therapeutic agent against esophageal carcinoma. The synthesized nerolidol-loaded zinc oxide and tin oxide NPs were fabricated and characterized for efficient delivery. However, much research was not focused on understanding the effect of nerolidol NPs against EC. Thus, the objective of our study is (1) to synthesize and characterize the nerolidol nanocomposite using zinc oxide and tin(II) nitrate hexahydrate and (2) to investigate esophageal carcinoma.

2 Materials and methods

2.1 Materials

Zinc nitrate hexahydrate ($Zn(NO_3)_2$)·$6H_2O$; MW: 297.48; 99%), tin(II) chloride ($SnCl_2$; Mw: 189.6; 98%), and NaOH were obtained from Sigma Chemicals (USA). Fetal bovine serum (FBS), nerolidol (MW: 222.37: 98%), penicillin/streptomycin, and RPMI-1640 medium were acquired from Merck Chemical Company (Germany). Dimethyl sulfoxide (DMSO) and other chemicals were acquired from Sigma (USA).

2.2 Synthesis of the nerolidol nanocomposite

The process involves dissolving 0.1 M of zinc nitrate ($Zn(NO_3)_2$) and 0.1 M of tin(II) nitrate hexahydrate ($Sn(NO_3)_2$·$6H_2O$) in 100 ml of deionized water. A 0.1 M NaOH solution was added dropwise to the metal mixture, followed by precipitation. The solution was heated with magnetic stirring for 4 h at around 80°C. The white precipitate formed was dried at 100°C. The ZnO–SnO_2 nanopowder was calcined at 600°C for 5 h to convert into ZnO–SnO_2 NPs.

Then, 500 mg of ZnO–SnO_2 NPs was dispersed in 5 mL of ethanol and then sonicated for 1 h. Next, 100 mg of nerolidol was added to the homogeneous ZnO–SnO_2 solution. The ZnO–SnO_2–nerolidol solution was stirred for 24 h at room temperature. The solution was centrifuged at 4°C for 15 min at 16,000 rpm. The solid ZnO–SnO_2–nerolidol was washed several times with distilled water and 100% ethanol to remove the unreacted materials. Finally, the ZnO–SnO_2–nerolidol solution was dried at 200°C for 2 h and used for further studies [19].

Zinc oxide and tin oxide intercalated with the bioactive compound nerolidol-based nanocomposite were characterized using various techniques, including UV–Vis spectroscopy, Fourier-transform infrared (FT-IR) spectroscopy, and scanning electron microscopy (SEM) [20].

2.3 UV-Vis spectroscopy

The synthesized nerolidol nanocomposite (intercalated with zinc oxide and tin oxide) was measured by UV–VIS spectrophotometer (UV-2000 PC spectrometer) at a wavelength ranging from 200 to 1,000 nm at a resolution of 0.5 nm. An absorption spectrum of synthesized nerolidol nanocomposite was obtained, which was plotted with the wavelength (at the *x*-axis) vs absorbance (at the *y*-axis) [8].

2.4 FT-IR analysis

The synthesized nerolidol nanocomposite was analyzed by FTIR (Perkin Elmer, Frontier, USA), which showed the presence of functional groups. The NPs were scanned from 4,000 to 400 cm^{-1} wavenumber in the transmission mode, and the spectrum was obtained from 50 scans with a resolution of 4 cm^{-1} [21].

2.5 X-ray diffraction (XRD)

XRD is a tool for characterizing the structural features of nerolidol nanocomposite, and XRD measurement was carried out using a Cu-Kα radiation source, and the instrument was operated at a voltage of 10 kV with a current of 30 mA with a scanning rate of 2°/min for 2θ between 0 and 40. The presence, crystalline nature, phase variety, and grain size of the synthesized nanocomposite were analyzed using XRD spectroscopy [22].

2.6 SEM

To obtain the morphology of the synthesized nanocomposite, a field emission scanning electron microscope (FESEM, CARL ZEISS SIPRA 55VP) coupled with an energy-dispersive X-ray (EDAX) analyzer (Oxford Instruments X-MAX (20 mm^2)) was operated at various voltages (5–20 kV). The shape, sizes, and atomic weight composition of the synthesized nanocomposite were analyzed [23].

2.7 Transmission electron microscopy (TEM)

TEM measurements were analyzed using a high-resolution TEM (JEOL 2010) with an accelerating voltage of 200 kV, and exposure was changed from 0 to 120 s [24].

2.8 Dynamic light scattering analysis

Dynamic light scattering was used to measure the surface charge, size, and also stability of the nanocomposite using Zetasizer Pro (Malvern Panalytical, UK). The data on the polydispersity and Z-average size of silver NPs were obtained. The images were captured using a Gatan Ultrascan digital camera [25].

2.9 Photoluminescence (PL)

PL emission spectra of the samples were recorded using a Shimadzu RF-5301 PC spectrofluorometer [25].

2.10 MTT assay

KYSE-150 (6000 cells) were cultured in 96-well plates in a culture medium maintained for 24 h. Then, the KYSE-150 cells were treated with different concentrations (2, 4, 8,16, 32, 64, and 128 µg/ml) of ZnO–SnO_2–nerolidol nanocomposite and exposed for 24 h in a CO_2 incubator at 37°C. Then, cells were mixed with 20 µL/mL MTT solution in each well carefully and incubated for 4 h at 37°C. To each well, 200 µL of 10% DMSO was added and allowed to mix for 30 min in a shaker until the formazan purple color precipitate was dissolved. The precipitation was measured at 595 nm absorbance using a VersaMax ELISA Microplate Reader (Molecular Devices Inc., Sunnyvale, CA, USA). Independent experiments were performed in triplicate [26].

2.11 Apoptosis analysis

2.11.1 Mitochondrial membrane potential

The morphological analysis of apoptotic cell death was performed by analyzing the alteration in intra-cellular mitochondrial membrane potential ($\Delta\Psi m$) using Rhodamine 123 in KYSE-150 cells. The cells were treated with IC_{50} doses of the nerolidol nanocomposite for 24 h. Rhodamine 123 was used to stain the cells for 5 min after washing with PBS. Again, the cells were washed with PBS, and the fluorescence microscope was used for examination of the stained cells using Nikon Eclipse Ti (Nikon Instruments Inc., NY, USA), and the effect of ZnO–SnO_2–nerolidol nanocomposite was compared with the untreated control [27].

2.11.2 Measurement of biochemical parameters

Superoxide dismutase (SOD), glutathione (GSH), and catalase (CAT) were determined using the colorimetric assay kits (Biovision Incorporation, CA, USA). Lipid peroxidation in the serum was evaluated by calculating the malondialdehyde (MDA) level after retorting MDA with thiobarbituric acid at wavelengths of 520–540 nm. SOD, CAT, and GSH were measured at 490 nm using a microplate reader

(Multiskan FC, Thermo Fischer Scientific; USA), and all these enzymatic antioxidants were expressed as units (U)/mg of protein [27].

2.12 Analysis of apoptotic proteins

The levels of caspases 3, 8, and 9 in cells were measured via ELISA (Biospes, China), according to the manufacturer's instructions. Briefly, the KYSE-150 cells were treated with an IC_{50} dose of the nerolidol nanocomposite and lysed according to the ELISA kit's instructions. The cell lysate contained caspases 3, 8, and 9 proteins, which were specifically bound to their primary antibodies and were detected using horseradish peroxidase (HRP)-conjugated secondary antibodies by measuring the absorbance at 450 nm using a microplate reader (Multiskan FC, Thermo Fischer Scientific, USA) [28].

2.13 Statistical analysis

Statistical analysis was performed using GraphPad Prism (version 6.01). The results are presented as mean ± SD. To determine if there were any differences between the groups, an ANOVA and the Tukey post-hoc tests were employed. Differences between means were considered statistically significant if $p < 0.05$.

3 Results

3.1 Characterization analysis

The UV-visible absorbance spectrum of the synthesized ZnO–SnO_2–nerolidol nanocomposite is shown in Figure 1. The absorption spectrum of the ZnO–SnO_2–nerolidol nanocomposite occurred at 288 nm. The FTIR spectra of the nerolidol nanocomposite are shown in Figure 2. In the synthesized nerolidol nanocomposite, peaks were observed at 570, 629, 960, 1,158, 1,454, 1,642, 2,922, and 3,397 cm^{-1}. The main characteristic peaks were found at 1,158, 1,454, 1,642, and 3,397 cm^{-1} and were attributed to the amino group (C–N) and CH_2 bend, the carboxylate group (COO–), the secondary amine group (NH_2), and the amine and hydroxyl stretch, respectively. Specifically, the nerolidol hydrocarbon chain peak was found at 2,922 cm^{-1}. The band between 945 and

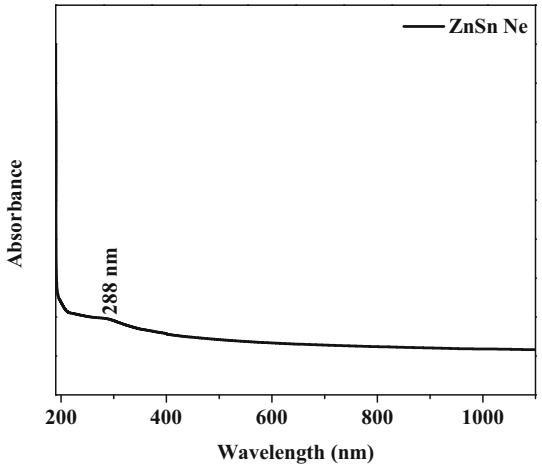

Figure 1: The UV-visible absorbance spectrum of the synthesized ZnO–SnO_2–nerolidol nanocomposite.

968 cm^{-1} was assigned to the OH vibration, and the peaks at 570 and 629 cm^{-1} were assigned to zinc-tin oxide-O stretching vibration. XRD is an important analytical parameter in understanding the molecular nature of nanocomposites, as shown in Figure 3. XRD patterns, which are indexed to the (110), (101), and (211) planes, confirmed the tetragonal structure of the synthesized nanocomposite and also indicated the presence of ZnO, SnO_2, and Ne. The diffraction peaks in the XRD patterns are of high intensity, which indicates the high crystallinity and high purity of the samples. The morphology of the ZnO–SnO_2–nerolidol nanocomposite was determined by FESEM analysis, as shown in Figure 4a. It showed cube crystalline agglomerate morphologies, and no rod or wire-shaped images were observed. EDAX analysis showed the presence of ZnO, SnO_2, C, and O in the ZnO–SnO_2–nerolidol nanocomposite, as shown in Figure 4b. The TEM analysis of the ZnO–SnO_2–nerolidol nanocomposite

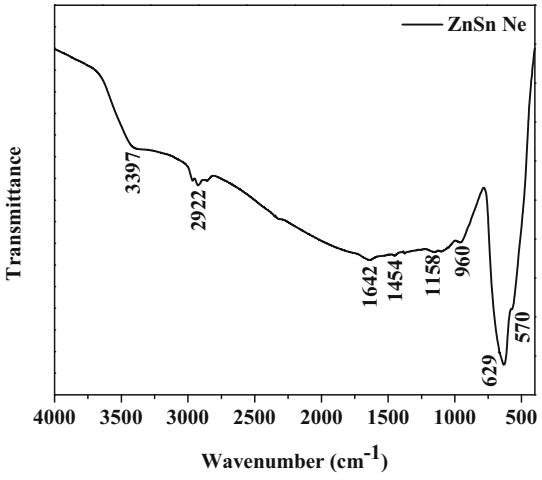

Figure 2: FTIR spectra of the ZnO–SnO_2–nerolidol nanocomposite.

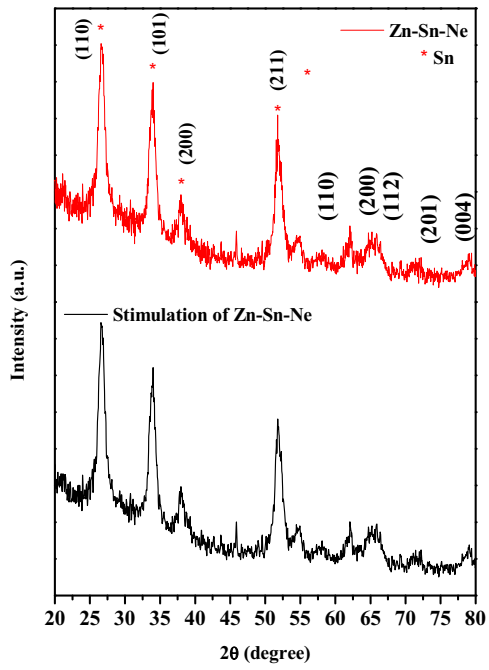

Figure 3: XRD patterns of the ZnO–SnO_2–nerolidol nanocomposite.

revealed the microsphere structure (Figure 5a–e), and SAED analysis revealed that the nanocomposite was polycrystalline in structures with irregular, partial, and incomplete rings (Figure 5f). The formation and particle size distribution of the ZnO–SnO_2–nerolidol nanocomposite was confirmed by dynamic light scattering, which revealed that the size of the nanocomposite was found to be 108.50 nm (Figure 6). PL spectra were used to investigate the electronic, optical, and photochemical properties of the NPs. Figure 7 shows that the PL spectra exhibit a sharp peak around 361 nm, indicating UV emission, and a broad spectrum around 425–478 nm, showing blue emission for the synthesized ZnO–SnO_2–nerolidol nanocomposite.

3.2 Cytotoxic effect of the ZnO–SnO_2–nerolidol nanocomposite against esophageal squamous cell carcinoma KYSE-150 cells

The cytotoxicity effect of the ZnO–SnO_2–nerolidol nanocomposite in KYSE-150 cells was tested using the MTT assay. Figure 8 shows the cell viability assay for KYSE-150 cells, which were treated with different concentrations of the ZnO–SnO_2–nerolidol nanocomposite ranging from 2 to 128 µg/mL. We observed a dose-dependent effect of the ZnO–SnO_2–nerolidol nanocomposite, and the IC_{50} concentration was found to be around 14.9 µg/mL. For further studies, IC25 and IC_{50} concentrations were selected to investigate apoptotic and oxidative stress potentials.

3.3 Effect of the ZnO–SnO_2–nerolidol nanocomposite on apoptosis

The KYSE-150 cells were stained using Rhodamine 123 stain and were observed under a fluorescence microscope to investigate the proapoptotic effect of the ZnO–SnO_2–nerolidol nanocomposite against KYSE-150 cells (Figure 9b). The apoptotic cells were dose-dependently enhanced in the ZnO–SnO_2–nerolidol nanocomposite-treated cells compared to the control KYSE-150 cells (Figure 9a). Additional dual staining provided information on various stages of apoptosis, such as necrosis, late apoptosis, and early apoptosis in the ZnO–SnO_2–nerolidol nanocomposite. The early-stage apoptotic cells indicated a granular pattern with yellow–green acridine orange nuclear stain, and the late-stage apoptotic cells exhibited orange nuclear EtBr stain; in addition, necrotic cells were distinguished with uneven orange-red fluorescence in the ZnO–SnO_2–nerolidol nanocomposite-treated KYSE-150 cells

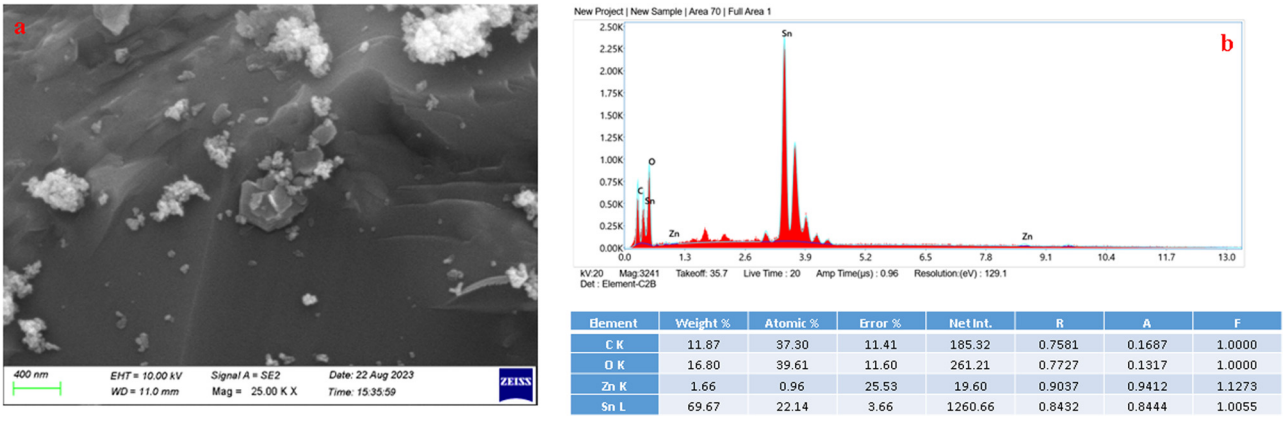

Element	Weight %	Atomic %	Error %	Net Int.	R	A	F
C K	11.87	37.30	11.41	185.32	0.7581	0.1687	1.0000
O K	16.80	39.61	11.60	261.21	0.7727	0.1317	1.0000
Zn K	1.66	0.96	25.53	19.60	0.9037	0.9412	1.1273
Sn L	69.67	22.14	3.66	1260.66	0.8432	0.8444	1.0055

Figure 4: The morphological analysis via FESEM (a) and elemental analysis via EDAX of the ZnO–SnO_2–nerolidol nanocomposite (b).

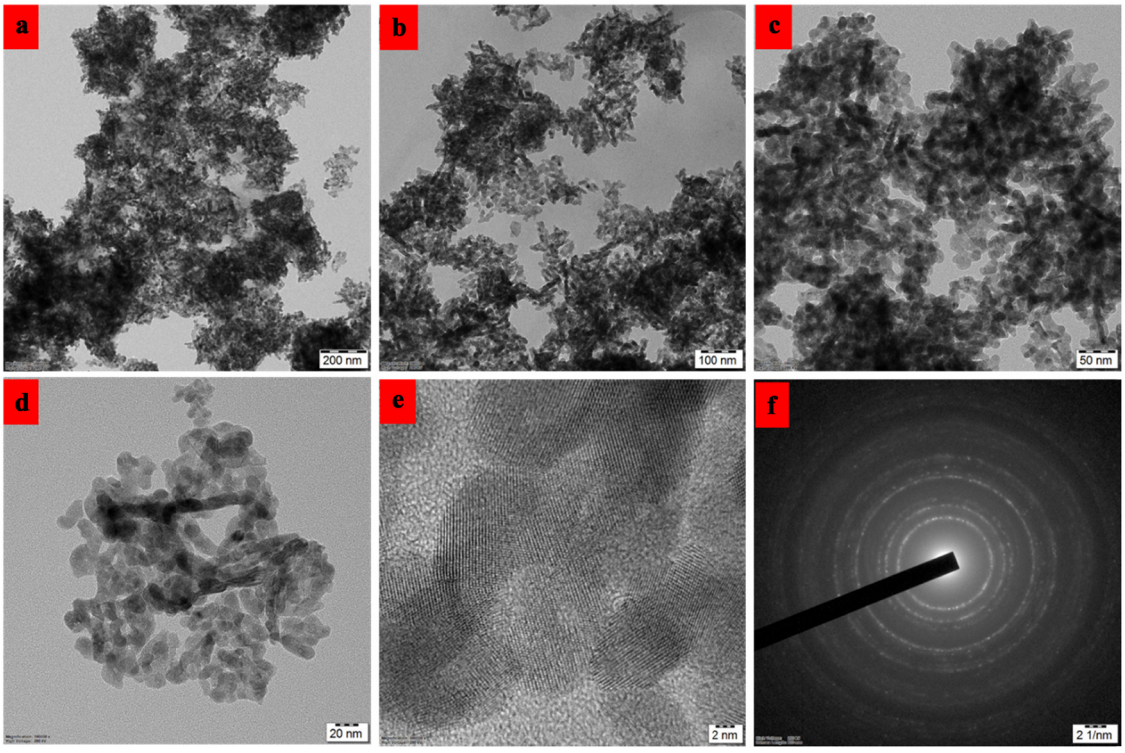

Figure 5: TEM analysis of the ZnO–SnO_2–nerolidol nanocomposite (a)–(e) and SAED analysis (f).

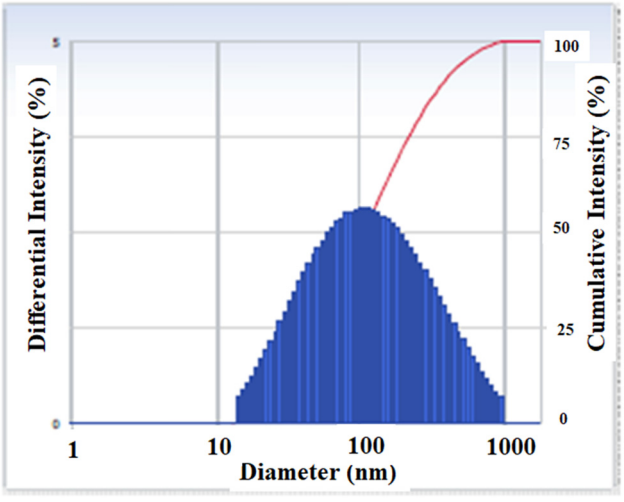

Figure 6: DLS analysis of the ZnO–SnO_2–nerolidol nanocomposite.

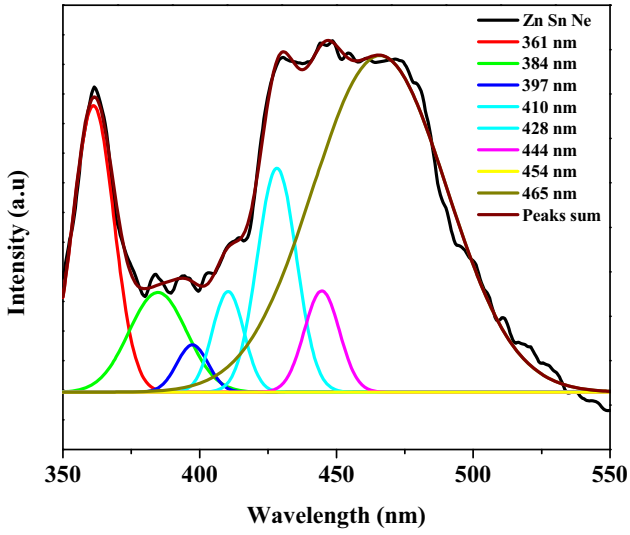

Figure 7: PL spectra of the ZnO–SnO_2–nerolidol nanocomposite.

dose-dependently. In this study, the cells were stained with Rhodamine 123 to investigate the mitochondrial membrane potential (Figure 9b). Upon treating the cells with the ZnO–SnO_2–nerolidol nanocomposite in KYSE-150 cells, the green fluorescence was enhanced dose-dependently, which depicted the depolarization of the mitochondrial membrane potential of the ZnO–SnO_2–nerolidol nanocomposite compared to that of control KYSE-150 cells.

3.4 Effect of the ZnO–SnO_2–nerolidol nanocomposite on lipid peroxidation and enzymatic antioxidants

The KYSE-150 cells treated with the ZnO–SnO_2–nerolidol nanocomposite were analyzed for lipid peroxidation, MDA (Figure 10a) level, and antioxidant enzyme activity (Figure 10b–d).

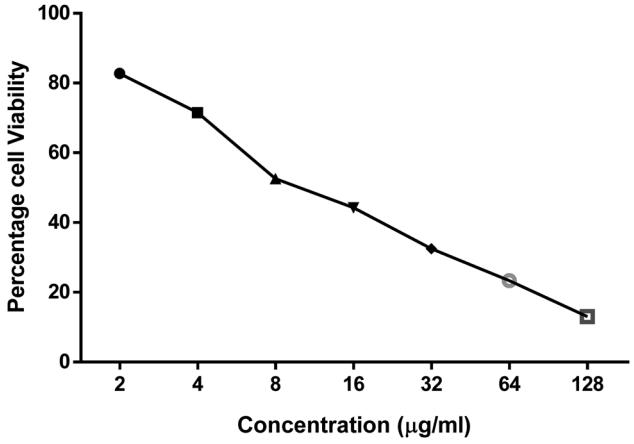

Figure 8: The cell viability assay for KYSE-150 cells treated with different concentrations of the ZnO–SnO_2–nerolidol nanocomposite ranging from 2 to 128 µg/mL.

There was a dose-dependent increase in the level of MDA in KYSE-150 cells treated with the ZnO–SnO_2–nerolidol nanocomposite, which indicated that the nanocomposite induced oxidative stress that leads to enhanced lipid peroxidation status. On the other hand, the antioxidant enzyme activities were tested, and we observed that SOD, CAT, and GSH were dose-dependently decreased in KYSE-150 cells treated with the ZnO–SnO_2–nerolidol nanocomposite when compared to control. The study investigates the effect of a ZnO–SnO_2–nerolidol nanocomposite on lipid peroxidation and enzymatic antioxidants in KYSE-150 cells.

The results suggest that an increase in MDA levels may indicate a defense response to oxidative stress, as increased free radicals cause oxidative damage (Figure 10a). The study also found that the nanocomposite caused dose-dependent decreases in SOD and GSH but increased CAT in KYSE-150 cells compared to the control group. These findings can indicate the nanocomposite's medicinal or toxicological aspects (Figure 10b–d).

3.5 Effect of the ZnO–SnO_2–nerolidol nanocomposite on apoptotic proteins

Figure 11 shows the levels of apoptotic proteins in both the control and the ZnO–SnO_2–nerolidol nanocomposite-treated KYSE-150 cells. Our ELISA data revealed that the pro-apoptotic proteins (caspases 3, 8, and 9) were found to be enhanced dose-dependently in the ZnO–SnO_2–nerolidol nanocomposite-treated KYSE-150 cells (Figure 11a–c) when compared to that of control cancer cells.

4 Discussion

Recently, nanomedicine has played a crucial role in the field of biomedicine, especially in the diagnosis and treatment of cancer. In our study, we synthesized the ZnO–SnO_2–nerolidol nanocomposite and characterized it using various techniques, including FTIR, FESEM, XRD, and EDAX. Next, the anticancer effect of the nanocomposite was found to be enhanced via stimulating lipid peroxidation and pro-apoptotic protein and by decreasing antioxidants in EC cells.

The UV-vis absorption spectra showed an absorption peak at 288 nm for the synthesized ZnO–SnO_2–nerolidol nanocomposite. In a previous study, it was reported that nerolidol-loaded chitosan–alginate NPs exhibited a broad peak between 230 and 280 nm; in addition, it was reported that diluting the nerolidol sample with a solvent like ethanol showed a band at 280 nm, which was consistent

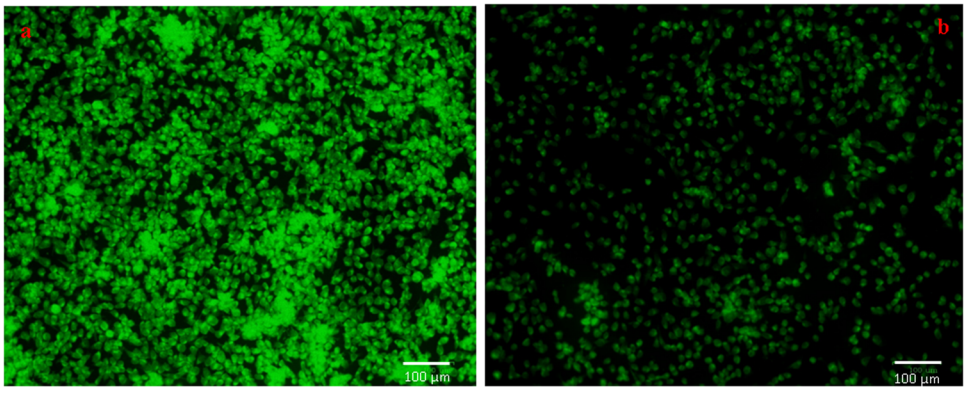

Figure 9: KYSE-150 cells stained using Rhodamine 123. (a) Control cancer cells and (b) the ZnO–SnO_2–nerolidol nanocomposite treatment at IC_{50} concentration.

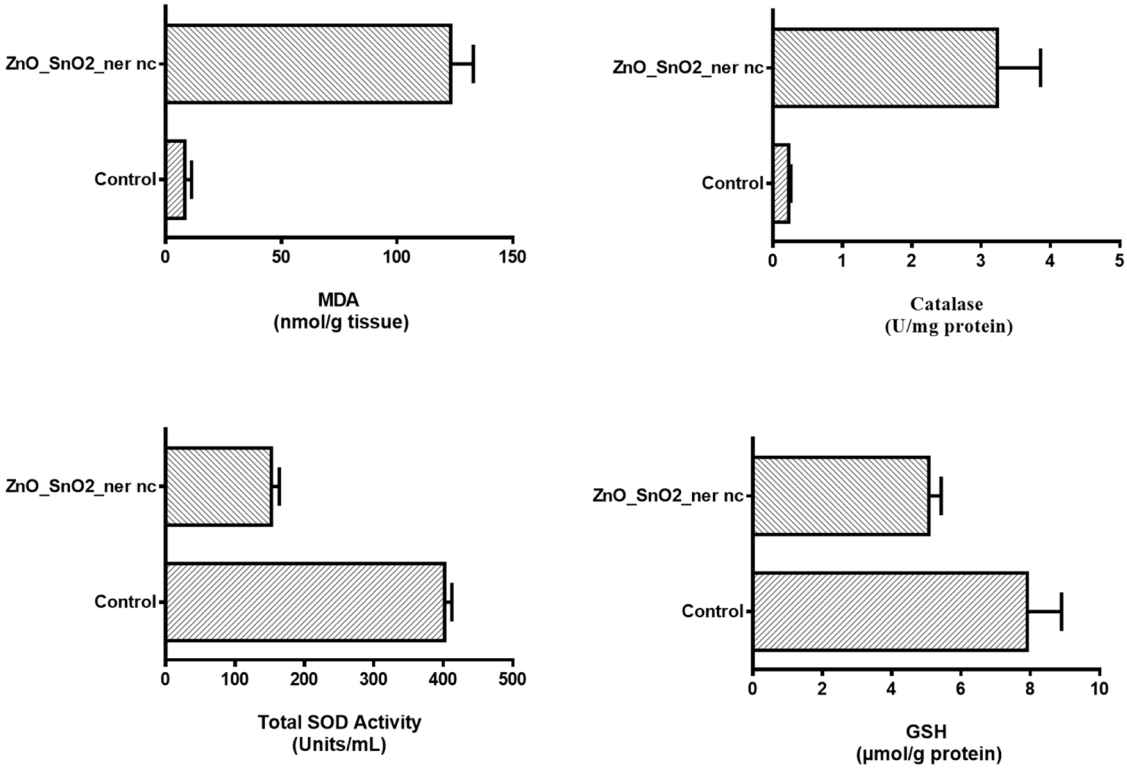

Figure 10: KYSE-150 cells treated with the ZnO–SnO_2–nerolidol nanocomposite and analyzed for lipid peroxidation, MDA level, and SOD, CAT, and GSH.

with our study [8]. Moreover, the absorption in the near UV region is due to the electronic transitions occurring in the sample [29]. FTIR spectroscopy helps to understand the interaction between functional groups and exhibit various peaks. In the synthesized nerolidol nanocomposite, we observed FTIR peaks at 570, 629, 960, 1,158, 1,454, 1,642, 2,922, and 3,397 cm^{-1}. The peaks confirmed that nerolidol successfully interacted with ZnO and SnO_2 oxide and it could be due to electrostatic interactions [30], and new peaks could be due to the weak physical and van der Waals interactions [31]. Our XRD data showed distinct characteristic peaks for the synthesized ZnO–SnO_2–nerolidol nanocomposite, and it showed that nerolidol is converted into the nanocomposite in the presence of ZnO and SnO_2 oxide, and sharp and strong peaks reflected well-ordered crystal structures of the synthesized nanomaterials. Consistent with our data, the crystalline nature of the NP showed characteristic peaks at 25.3°, 37.7°, 47.5°, 54.9°, 63.7°, 68.7°, 70.6°, and 75.5° [32]. Our FESEM data revealed that the ZnO–SnO_2–nerolidol nanocomposite exhibited spherical and cuboidal-shaped structures. In support of our results, in another study, it was shown that nerolidol-loaded chitosan–alginate NPs exhibited spherical-like particle morphology [8]. In our study, EDAX showed the elemental composition of the ZnO–SnO_2–nerolidol nanocomposite and confirmed the presence of ZnO, SnO_2, C, and O. Similar to our results, nerolidol gold NPs exhibited elemental composition upon EDAX analysis [33]. Morphology was assessed using TEM, and our data showed spherical-shaped ZnO–SnO_2–nerolidol nanocomposite, which was consistent with the results of Baldissera et al. [34], who reported that nerolidol formed a nanosphere and suppressed hepatic cellular damage and modulated bioenergetics. Moreover, SAED data of the ZnO–SnO_2–nerolidol nanocomposite were in agreement with the XRD data,

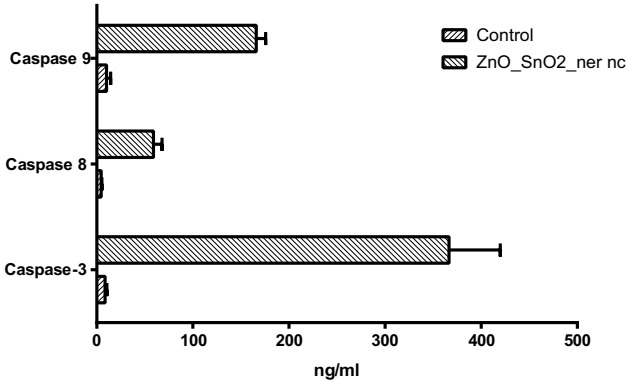

Figure 11: KYSE-150 cells treated with the ZnO–SnO_2–nerolidol nanocomposite and analyzed for pro-apoptotic proteins, caspases 3, 8, and 9.

indicating the crystalline nature and the ring formation due to the merging of diffraction spots that are formed from a large number of layers in the nanocomposite samples [35]. Our DLS showed the average diameter of the ZnO–SnO_2–nerolidol nanocomposite as 108 nm. Similar to our data, in another study, vesicles carrying nerolidol showed average diameters of 132.3 nm, while the vesicles were 185.46 nm [36].

Our PL data on the ZnO–SnO_2–nerolidol nanocomposite showed UV emission, which could be due to the recombination of the free excitons through an exciton–exciton collision process, and the blue emission band showed oxygen vacancies. Koshy et al. [37] reported that the band edge-free excitons are involved in the formation of the visible emission peaks at 418, 449, 485, 513, and 532 nm, while Kang et al. [38] reported that PL data in the range of 400–550 nm are due to surface oxygen vacancies. The intercalation of nerolidol with the ZnO–SnO_2 NPs can be confirmed through various characterization techniques. FTIR can detect changes in the vibrational modes of functional groups, such as shifts in nerolidol's characteristic peaks and new peaks or changes in the peak intensity. XRD can reveal changes in the crystalline structure of the ZnO–SnO_2 NPs upon intercalation, such as changes in the diffraction patterns or structural modifications. SEM and TEM can provide morphological evidence and insights into the distribution of nerolidol within the NPs. DLS analysis can measure the particle size distribution and surface charges, indicating nerolidol incorporation. These techniques provide comprehensive evidence of successful intercalation and the formation of the nerolidol-loaded ZnO–SnO_2 nanocomposite.

The study explores environmentally friendly synthesis methods for MgO NPs coated with chitosan using crab and shrimp shells. The resulting NPs exhibit varying particle sizes and shapes, with 89% efficient photocatalytic activity, strong radical scavenging capacity, and high total antioxidant capacity [39]. NPs have shown potential in wound healing by promoting antibacterial, anti-inflammatory, and angiogenic activities and their effectiveness as carriers for therapeutic compounds [40]. A fast method for removing DOX from aqueous samples was developed using ZnO/Ce-LDH as an efficient adsorbent, achieving a maximum capacity of 1,297 mg g^{-1} [41]. Hospital pharmaceutical waste, including antibiotics, chemicals, and hormones, poses health concerns. NPs like nanomaterials, carbon nanotubes, and nanofillers are being investigated for waste removal effectiveness [42]. The damaged mitochondrial membrane potential is the earliest event of apoptosis, followed by the activation of apoptotic caspases that eventually lead to DNA fragmentation [43]. In colorectal cancer cells, nerolidol-loaded solid lipid NPs rapidly internalized and also retained inside the cells and subsequently enhanced apoptosis via activating the caspase cascade [44] (Table 1).

The study of nanocomposites, particularly ZnO–SnO_2–nerolidol, focuses on their impact on oxidative stress markers and apoptosis-related proteins. The nanocomposite may reduce MDA, a marker of lipid peroxidation, and upregulate SOD activity, suggesting enhanced antioxidant defense mechanisms [56,57]. Increased catalase activity suggests the nanocomposite's role in mitigating oxidative

Table 1: Studies evaluating the use of ZnO/SnO_2 NPs in anticancer research along with other catalysts

Combination	Mechanism/effect	Key findings
ZnO/SnO_2 and gold nanoparticles (AuNPs)	Enhanced ROS generation and improved cellular uptake	Improved photothermal and photodynamic therapy and increased cytotoxicity toward cancer cells [45]
ZnO/SnO_2 and silver nanoparticles (AgNPs)	Increased ROS production and enhanced apoptosis induction	Significant anticancer activity with combined antimicrobial and anticancer properties [46]
ZnO/SnO_2 and graphene oxide (GO)	High surface area, enhanced drug loading, and ROS generation	Improved anticancer efficacy and increased cytotoxicity toward cancer cells [47]
ZnO/SnO_2 and carbon nanotubes (CNTs)	High mechanical strength, conductivity, enhanced delivery, and ROS levels	Better targeting and killing of cancer cells, potential in anticancer applications [48]
ZnO/SnO_2 and chitosan	Biocompatibility, targeted drug delivery, and sustained release	Enhanced anticancer activity and improved therapeutic outcomes against cancer cells [49]
ZnO/SnO_2 and polyethylene glycol (PEG)	Improved biocompatibility, prolonged circulation time, and better tumor accumulation	Enhanced anticancer activity with reduced toxicity to normal cells [50]
ZnO/SnO_2 and iron oxide (Fe_3O_4)	Magnetic properties for targeted delivery and enhanced ROS generation	Significant anticancer effects and apoptosis induction in cancer cells using external magnetic fields [51]
ZnO/SnO_2 and copper oxide (CuO)	Synergistic ROS production and improved drug delivery	Enhanced anticancer activity through combined cytotoxic effects [52]
ZnO/SnO_2 and doxorubicin	Improved drug delivery, increased intracellular accumulation, and ROS-mediated damage	Enhanced cytotoxicity towards cancer cells and better therapeutic effects [53]
ZnO/SnO_2 and curcumin	Synergistic ROS production, anti-inflammatory, and anticancer properties of curcumin	Enhanced overall therapeutic potential against cancer cells and improved anticancer properties [54,55]

stress by decomposing hydrogen peroxide. Enhanced levels of GSH indicate improved cellular redox status and detoxification capability [58,59]. Caspase 3, a key apoptotic protein, may induce apoptosis in cells, potentially targeting cancer cells. Caspases 8 and 9 are involved in the extrinsic and intrinsic apoptotic pathways, potentially due to mitochondrial damage or stress [60,61]. The nanocomposite's effects may be mediated through antioxidant properties, enzyme modification, and apoptotic pathways. The ZnO–SnO_2–nerolidol nanocomposite may reduce MDA levels, enhance antioxidant defense by increasing SOD, CAT, and GSH activities, and induce apoptosis through increased caspases 3, 8, and 9, potentially targeting esophageal squamous cell carcinoma of KYSE-150 cells.

In anti-cancer research, apoptosis is one of the crucial mechanisms that receive a lot of attention as it is necessary for the eradication of cancerous cells via modulating anti-apoptotic and proapoptotic proteins [60]. In the current study, our MTT assay showed the cytotoxic effect of the ZnO–SnO_2–nerolidol nanocomposite in a dose-dependent manner. Additionally, Rhodamine revealed that the ZnO–SnO_2–nerolidol nanocomposite stimulated oxidative stress and apoptosis in KYSE-150 cells. Caspases are crucial proteins involved in the regulation of programmed cell death; however, inadequate activation of caspases can lead to carcinogenesis. In this regard, caspases are categorized into initiator caspases (caspases 8 and 9) and killer caspases (caspases 3, 6, and 7) [61]. Thus, in our study, we expect that our nanocomposite can internalize and form agglomeration that would kill cancer cells and additionally might activate the caspase cascade to induce apoptosis against EC cells.

5 Conclusion

In conclusion, we synthesized the ZnO–SnO_2–nerolidol nanocomposite and characterized it using various techniques, including FESEM, FTIR, XRD, UV, and PL. The spectral analysis of the synthesized ZnO–SnO_2–nerolidol nanocomposite indicates the presence of zinc–tin oxide bonding patterns. The XRD diffraction pattern confirms the tetragonal structure of the synthesized nanocomposite and the presence of ZnO, SnO_2, and Ne molecules. The nanocomposite ZnO–SnO_2–nerolidol was observed to have a molecular architecture and contained ZnO, SnO_2, C, and O. We tested the efficacy of the ZnO–SnO_2–nerolidol nanocomposite against esophageal squamous carcinoma and found that nanocomposites effectively inhibited proliferation and induced apoptosis via the mitochondrial pathway and ultimately enhanced the caspase cascade that eventually leads to DNA fragmentation. Based on our data, we suggest that it could be used as an effective treatment strategy against esophageal carcinoma. However, understanding molecular circuits targeting apoptosis needs to be investigated and also detailed analysis under *in vivo* conditions is still warranted.

Acknowledgments: The authors are thankful to the Fourth Hospital of Hebei Medical University and Linxi County People's Hospital for their support.

Funding information: This research received no external funding.

Author contributions: Conceptualization, methodology, and funding acquisition, Kun Gao; software and formal analysis, Zujian Chen; investigation and resources, Na Zhang; data curation and writing – original draft preparation, and writing – review and editing, Pu Jiang. All authors have read and agreed to the published version of the manuscript.

Conflict of interest: The authors declare no conflict of interest.

Ethical approval: The conducted research is not related to either human or animals use.

Data availability statement: The data that support the findings of this study are available on request from the corresponding author.

References

[1] Chen Y, Huang K, Ding X, Tang H, Xu Z. Magnolol inhibits growth and induces apoptosis in esophagus cancer KYSE-150 cell lines via the MAP kinase pathway. J Thorac Dis. 2019 Jul;11(7):3030–8. doi: 10.21037/jtd.2019.07.46. PMID: 31463132; PMCID: PMC6688004.

[2] Pennathur A, Gibson MK, Jobe BA, Luketich JD. Oesophageal carcinoma. Lancet. 2013 Feb;381(9864):400–12. doi: 10.1016/S0140-6736(12)60643-6. PMID: 23374478.

[3] Chen R, Zheng R, Zhang S, Wang S, Sun K, Zeng H, et al. Patterns and trends in esophageal cancer incidence and mortality in China: An analysis based on cancer registry data. J Natl Cancer Cent. 2023;3:21–7. doi: 10.1016/j.jncc.2023.01.002.

[4] Mao WM, Zheng WH, Ling ZQ. Epidemiologic risk factors for esophageal cancer development. Asian Pac J Cancer Prev. 2011;12:2461–6.

[5] Yan X, Duan H, Ni Y, Zhou Y, Wang X, Qi H, et al. Tislelizumab combined with chemotherapy as neoadjuvant therapy for surgically resectable esophageal cancer: A prospective, single-arm, phase II study (TD-NICE). Int J Surg. 2022;103:106680. doi: 10.1016/j.ijsu.2022.106680.

[6] Rao PV, Nallappan D, Madhavi K, Rahman S, Jun Wei L, Gan SH. Phytochemicals and biogenic metallic nanoparticles as anticancer agents. Oxid Med Cell Longev. 2016;2016:3685671. doi: 10.1155/2016/3685671. Epub 2016 Feb 23, PMID: 27057273; PMCID: PMC4781993.
[7] Ferreira FM, Palmeira CM, Oliveira MM, Santos D, Simões AM, Rocha SM, et al. Nerolidol effects on mitochondrial and cellular energetics. Toxicol Vitro. 2012;26:189–96.
[8] Ahmad RM, Greish YE, El-Maghraby HF, Lubbad L, Makableh Y, Hammad FT. Preparation and characterization of blank and nerolidol-loaded chitosan-alginate nanoparticles. Nanomaterials (Basel). 2022 Apr;12(7):1183. doi: 10.3390/nano12071183. PMID: 35407300; PMCID: PMC9000846.
[9] Chan WK, Tan LTH, Chan KG, Lee LH, Goh BH. Nerolidol: A sesquiterpene alcohol with multi-faceted pharmacological and biological activities. Molecules. 2016;21:529. doi: 10.3390/molecules21050529.
[10] Iqbal J, Abbasi BA, Yaseen T, Zahra SA, Shahbaz A, Shah SA, et al. Green synthesis of zinc oxide nanoparticles using Elaeagnus angustifolia L. leaf extracts and their multiple in vitro biological applications. Sci Rep. 2021;11(1):20988. doi: 10.1038/s41598-021-99839-z.
[11] Hahm JI. Biomedical detection via macro- and nano-sensors fabricated with metallic and semiconducting oxides. J Biomed Nanotechnol. 2013 Jan;9(1):1–25. doi: 10.1166/jbn.2013.1468. PMID: 23627064; PMCID: PMC3766318.
[12] Ibraheem S, Kadhim AA, Kadhim KA, Kadhim IA, Jabir M. Zinc oxide nanoparticles as diagnostic tool for cancer cells. Int J Biomater. 2022 Nov;2022:2807644. doi: 10.1155/2022/2807644. PMID: 36387955; PMCID: PMC9646305.
[13] Bisht G, Rayamajhi S. ZnO nanoparticles: a promising anticancer agent. Nanobiomedicine. 2016 Jan;3:9. doi: 10.5772/63437. PMID: 29942384; PMCID: PMC5998263.
[14] Iqbal MJ, Javed Z, Sadia H, Mehmood S, Akbar A, Zahid B, et al. Targeted therapy using nanocomposite delivery systems in cancer treatment: highlighting miR34a regulation for clinical applications. Cancer Cell Int. 2023;23(1):84. doi: 10.1186/s12935-023-02929-3.
[15] Sun L, Liu H, Ye Y, Lei Y, Islam R, Tan S, et al. Smart nanoparticles for cancer therapy. Signal Transduct Target Ther. 2023;8(1):418. doi: 10.1038/s41392-023-01642-x.
[16] Alhoqail WA, Alothaim AS, Suhail M, Iqbal D, Kamal M, Asmari MM, et al. Husk-like zinc oxide nanoparticles induce apoptosis through ROS generation in epidermoid carcinoma cells: effect of incubation period on sol-gel synthesis and anti-cancerous properties. Biomedicines. 2023 Jan;11(2):320. doi: 10.3390/biomedicines11020320. PMID: 36830857; PMCID: PMC9953567.
[17] Alshahateet SF, Altarawneh RM, Al-Tawarh WM, Al-Trawneh SA, Al-Taweel S, Azzaoui K, et al. Catalytic green synthesis of Tin(IV) oxide nanoparticles for phenolic compounds removal and molecular docking with EGFR tyrosine kinase. Sci Rep. 2024;14(1):6519. doi: 10.1038/s41598-024-55460-4.
[18] Guo Y, Yongli Z, Xiaobo Z, Shanshan S, Bai Q. Exploring the anticancer effects of tin oxide nanoparticles synthesized by pulsed laser ablation technique against breast cancer cell line through down-regulation of PI3K/AKT/MTOR signaling pathway. Arab J Chem. 2021;14(7):103212. doi: 10.1016/j.arabjc.2021.103212. Accessed May 19, 2024.
[19] Indumathi T, Suriyaprakash J, Alarfaj AA, Hirad AH, Jaganathan R, Mathanmohun M. Synergistic effects of CuO/TiO2 -chitosan-farnesol nanocomposites: Synthesis, characterization, antimicrobial, and anticancer activities on melanoma cells SK-MEL-3. J Basic Microbiol. 2024 Feb;64(2):e2300505. doi: 10.1002/jobm.202300505. Epub 2023 Nov 21 PMID: 37988658.
[20] González C, Vilaplana JM, Serrano A. Monte-Carlo evaluation of uncertainties of UV spectra measured with brewer spectroradiometers. J Geophys Res Atmos. 2023;128(24):e2023JD039500.
[21] Valle AL, Silva ACA, Dantas NO, Sabino-Silva R, Melo FCC, Moreira CS, et al. Application of ZnO nanocrystals as a surface-enhancer FTIR for glyphosate detection. Nanomaterials (Basel). 2021 Feb;11(2):509. doi: 10.3390/nano11020509.PMID: 33671396; PMCID: PMC7922178.
[22] Lam NH, Smith RP, Le N, Thuy CTT, Tamboli MS, Tamboli AM, et al. Evaluation of the structural deviation of Cu/Cu2O nanocomposite using the X-ray diffraction analysis methods. Crystals. 2022;12(4):566. doi: 10.3390/cryst12040566.
[23] Ang BC, Yaacob II, Nurdin I. Investigation of nanocomposite by FESEM and TEM. J Nanomater. 2013;2013:6. Article ID 980390. 6. doi: 10.1155/2013/980390.
[24] Chen X, Zhou L, Wang P, Cao H, Miao X, Wei F, et al. Effects associated with nanostructure fabrication using in situ liquid cell TEM technology. Nanomicro Lett. 2015;7(4):385–91. doi: 10.1007/s40820-015-0054-4. Epub 2015 Jul 28. PMID: 30464986; PMCID: PMC6223903 .
[25] Malm AV, Corbett JCW. Improved dynamic light scattering using an adaptive and statistically driven time-resolved treatment of correlation data. Sci Rep. 2019 Sep;9(1):13519. doi: 10.1038/s41598-019-50077-4. Erratum: Sci Rep. 2024 Jan;14(1) 2021. PMID: 31534186; PMCID: PMC6751167.
[26] Hu A, Abdullah AA, Abdurahman HH, Vishnu PV, Krishna MS, Samer HH, et al. Chitosan-sodium alginate-polyethylene glycol-crocin nanocomposite treatment inhibits esophageal cancer KYSE-150 cell growth via inducing apoptotic cell death. Arab J Chem. 2022;15(6):103844. Accessed May 18, 2024. doi: 10.1016/j.arabjc.2022.103844.
[27] Gusti AMT, Qusti SY, Alshammari EM, Toraih EA, Fawzy MS. Antioxidants-related superoxide dismutase (SOD), catalase (CAT), glutathione peroxidase (GPX), glutathione-S-transferase (GST), and nitric oxide synthase (NOS) gene variants analysis in an obese population: a preliminary case-control study. Antioxid (Basel). 2021 Apr;10(4):595. doi: 10.3390/antiox10040595. PMID: 33924357; PMCID: PMC8070436.
[28] Shi X, Bian X, Huang T, Wen B, Zhao L, Mu H, et al. Azoxystrobin induces apoptosis of human esophageal squamous cell carcinoma KYSE-150 cells through triggering of the mitochondrial pathway. Front Pharmacol. 2017;8:277. doi: 10.3389/fphar.2017.00277.
[29] Farahmandjou M, Soflaee F. Synthesis and characterization of α-Fe2O3 nanoparticles by simple co-precipitation method. Phys Chem Res. 2015;3(3):191–6.
[30] Vishnuvardhanaraj G, Bharathidasan G, Tamilvedan D, Karthikeyan C. Biocidal properties of Chitosan-encapsulated ternary titanium dioxide-nickel oxide-copper oxide hybrid nanomaterials were prepared via a facile one-pot precipitation process. BioNanoSci. 2023;13:1863–9.
[31] Bonn M, Hunger J. Between a hydrogen and a covalent bond. Science. 2021;371(6525):123–4. doi: 10.1126/science.abf3543.
[32] Sedky NK, Mahdy NK, Abdel-Kader NM, Abdelhady MMM, Maged M, Allam AL, et al. Facile sonochemically-assisted bioengineering of titanium dioxide nanoparticles and deciphering their potential in treating breast and lung cancers: biological, molecular, and computational-based investigations. RSC Adv. 2024 Mar;14(12):8583–8601. doi: 10.1039/d3ra08908h. PMID: 38487521; PMCID: PMC10938292.

[33] Yu J, Wang X, Li Y, Huang X, Luo X, He X. Synthesis of nerolidol functionalized gold nanoparticles for wound regeneration in people with diabetic foot ulcers in nursing care management. Sci Adv Mater. 2018;10(12):1775–81.
[34] Baldissera MD, Souza CF, Velho MC, Bassotto VA, Ourique AF, Da Silva AS, et al. Nanospheres as a technological alternative to suppress hepatic cellular damage and impaired bioenergetics caused by nerolidol in Nile tilapia (Oreochromis niloticus). Naunyn-Schmiedeberg's Arch Pharmacol. 2020;393(5):751–9. doi: 10.1007/s00210-020-01824-2.
[35] Krishnamoorthy K, Veerapandian M, Yun K, Kim SJ. The chemical and structural analysis of graphene oxide with different degrees of oxidation. Carbon. 2013;53:38–49.
[36] Fonseca Bezerra C, de Alencar Júnior JG, de Lima Honorato R, Dos Santos ATL, Pereira da Silva JC, Silva TGD, et al. Antifungal properties of nerolidol-containing liposomes in association with fluconazole. Membr (Basel). 2020 Aug;10(9):194. doi: 10.3390/membranes10090194. PMID: 32825411; PMCID: PMC7558210.
[37] Koshy J, Samuel MS, Chandran A, George KC. Optical properties of CuO nanoparticles. AIP Conference Proceedings. Vol. 1391, No. 1. American Institute of Physics; 2011, Oct. p. 576–8.
[38] Kang X, Berberidou C, Galeckas A, Bazioti C, Sagstuen E, Norby T, et al. Visible light-driven photocatalytic decolorization and disinfection of water employing reduced TiO2 nanopowders. Catalysts. 2021;11(2):228.
[39] Amor IB, Hemmami H, Laouini SE, Ahmed S, Mohammed HA, Abdullah JAA, et al. Enhancing oxidant and dye scavenging through MgO-based chitosan nanoparticles for potential antioxidant coatings and efficient photocatalysts. Biomass Conv Bioref. 2023. doi: 10.1007/s13399-023-04923-1.
[40] Hamed SH, Azooz EA, Al-Mulla EAJ. Nanoparticles-assisted wound healing: A review. Nano Biomed Eng. 2023;15(4):425–35. doi: 10.26599/NBE.2023.9290039.
[41] Ramezani AM, Panah FA, Dokoohaki MH, Azooz EA, Ahmadi R, Nazari S. Zn/Ce-layered double hydroxide for adsorptive removal of doxycycline from water. Mater Chem Phys. 2024;318:129223. Accessed May 18, 2024. doi: 10.1016/j.matchemphys.2024.129223.
[42] Al-Toriahi AKM, Azooz EA, Al-Mulla EAJ. Metal nanoparticles and nano-filters for the disposal of hospital waste: a review. Nano Biomed Eng. 2023;15(2):179–90. doi: 10.26599/NBE.2023.9290017.
[43] Lu J, Wu L, Wang X, Zhu J, Du J, Shen B. Detection of mitochondria membrane potential to study CLIC4 knockdown-induced HN4 cell apoptosis in vitro. J Vis Exp. 2018 Jul;137:56317. doi: 10.3791/56317. PMID: 30080203; PMCID: PMC6126487.
[44] Parvez S, Karole A, Mudavath SL. Fabrication, physicochemical characterization, and In vitro anticancer activity of nerolidol encapsulated solid lipid nanoparticles in the human colorectal cell line. Colloids Surf B Biointerfaces. 2022 Jul;215:112520. doi: 10.1016/j.colsurfb.2022.112520. Epub 2022 Apr 26. PMID: 35489319.
[45] Jeong EH, Jung G, Hong CA, Lee H. Gold nanoparticle (AuNP)-based drug delivery and molecular imaging for biomedical applications. Arch Pharm Res. 2014 Jan;37(1):53–9. doi: 10.1007/s12272-013-0273-5. Epub 2013 Nov 12. PMID: 24214174.
[46] Tripathi DK, Singh S, Singh S, Srivastava PK, Singh VP, Singh S, et al. Nitric oxide alleviates silver nanoparticles (AgNps)-induced phytotoxicity in Pisum sativum seedlings. Plant Physiol Biochem. 2017 Jan;110:167–77. doi: 10.1016/j.plaphy.2016.06.015. Epub 2016 Jun 15. PMID: 27449300.
[47] Kim T, Parale VG, Jung HN, Kim Y, Driss Z, Driss D, et al. Facile synthesis of SnO_2 aerogel/reduced graphene oxide nanocomposites via in situ annealing for the photocatalytic degradation of methyl orange. Nanomaterials (Basel). 2019 Mar;9(3):358. doi: 10.3390/nano9030358. PMID: 30836632; PMCID: PMC6473939.
[48] Zhang D, Tang Y, Zhang C, Dong Q, Song W, He Y. One-step synthesis of SnO2/carbon nanotube nanonests composites by direct current arc-discharge plasma and its application in lithium-ion batteries. Nanomaterials. 2021;11(11):3138. doi: 10.3390/nano11113138.
[49] Kafi AKM, Alim S, Jose R, Yusoff MM. Hemoglobin immobilization on multiporous nanofibers of SnO_2 and chitosan composite for hydrogen peroxide sensing. J Nanosci Nanotechnol. 2019 Apr;19(4):2027–33. doi: 10.1166/jnn.2019.15465. PMID: 30486943.
[50] Chen H, Govindasamy C, Oh DH, Chelliah R, Ramamoorthy A, Rengarajan T, et al. Synthesis of SnO_2-sodium alginate-polyethylene glycol-crocin nanocomposite for enhanced antimicrobial and anticancer activity. J Drug Delivery Sci Technol. 2024;93:105449. Accessed May 20, 2024. doi: 10.1016/j.jddst.2024.105449.
[51] Dorniani D, Hussein MZ, Kura AU, Fakurazi S, Shaari AH, Ahmad Z. Preparation of Fe_3O_4 magnetic nanoparticles coated with gallic acid for drug delivery. Int J Nanomed. 2012;7:5745–56. doi: 10.2147/IJN.S35746. Epub 2012 Nov 12. PMID: 23166439; PMCID: PMC3500033.
[52] Thevenot P, Cho J, Wavhal D, Timmons RB, Tang L. Surface chemistry influences cancer killing effect of TiO2 nanoparticles. Nanomedicine. 2008 Sep;4(3):226–36. doi: 10.1016/j.nano.2008.04.001, Epub 2008 May 23. PMID: 18502186; PMCID: PMC2597280.
[53] Mishra P, Ahmad A, Al-Keridis LA, Alshammari N, Alabdallah NM, Muzammil K, et al. Doxorubicin-conjugated zinc oxide nanoparticles, biogenically synthesised using a fungus aspergillus niger, exhibit high therapeutic efficacy against lung cancer cells. Molecules. 2022 Apr;27(8):2590. doi: 10.3390/molecules27082590. PMID: 35458790; PMCID: PMC9030660.
[54] Ahmed MA, Al-Zaqri N, Alsalme A, Glal AH, Esa M. Rapid photocatalytic degradation of RhB dye and photocatalytic hydrogen production on novel curcumin/SnO_2 nanocomposites through direct Z-scheme mechanism. J Mater Sci: Mater Electron. 2020;31:19188–203. doi: 10.1007/s10854-020-04455-8.
[55] Beyene AM, Moniruzzaman M, Karthikeyan A, Min T. Curcumin nanoformulations with metal oxide nanomaterials for biomedical applications. Nanomaterials. 2021;11(2):460. doi: 10.3390/nano11020460.
[56] Hurşitoğlu O, Orhan FÖ, Kurutaş EB, Doğaner A, Durmuş HT, Kopar H. Diagnostic performance of increased malondialdehyde level and oxidative stress in patients with schizophrenia. Noro psikiyatri arsivi. 2021;58(3):184–8. doi: 10.29399/npa.27372.
[57] Jomova K, Alomar SY, Alwasel SH, Nepovimova E, Kuca K, Valko M. Several lines of antioxidant defense against oxidative stress: antioxidant enzymes, nanomaterials with multiple enzyme-mimicking activities, and low-molecular-weight antioxidants. Arch Toxicol. 2024;98:1323–67. doi: 10.1007/s00204-024-03696-4.
[58] Nandi A, Yan LJ, Jana CK, Das N. Role of catalase in oxidative stress- and age-associated degenerative diseases. Oxid Med Cell Longev. 2019;2019:9613090. doi: 10.1155/2019/9613090.
[59] Rasheed Z. Therapeutic potentials of catalase: Mechanisms, applications, and future perspectives. Int J health Sci. 2024;18(2):1–6.
[60] McIlwain DR, Berger T, Mak TW. Caspase functions in cell death and disease. Cold Spring Harb Perspect Biol. 2013;5(4):a008656. doi: 10.1101/cshperspect.a008656.
[61] Boice A, Bouchier-Hayes L. Targeting apoptotic caspases in cancer. Biochimica Et Biophysica Acta (BBA) – Mol Cell Res. 2020;1867(6):118688. Accessed June 8, 2024. doi: 10.1016/j.bbamcr.2020.118688.